

References and Notes

1. E. S. Jr. Connolly *et al.*, *Circ. Res.* **81**, 304 (1997).
2. E. S. Jr. Connolly *et al.*, *J. Clin. Invest.* **97**, 209 (1996).
3. T. F. Choudhri *et al.*, *ibid.* **102**, 1301 (1998).
4. A. Afagh, B. J. Cummings, D. H. Cribbs, C. W. Cotman, A. J. Tenner, *Exp. Neurol.* **138**, 22 (1996); S. A. Johnson *et al.*, *Neurobiol. Aging* **13**, 641 (1992).
5. A. R. Korotzer *et al.*, *ibid.* **134**, 214 (1995).
6. Y. Naka, H. C. Marsh, S. M. Scesney, M. C. Oz, D. J. Pinsky, *Transplantation* **64**, 1248 (1997); M. Pemberton, G. Anderson, V. Vetvicka, D. E. Justus, G. D. Ross, *J. Immunol.* **150**, 5104 (1993); R. E. Chavez-Cartaya, G. P. DeSola, L. Wright, N. V. Jamieson, D. J. White, *Transplantation* **59**, 1047 (1995); J. Hill *et al.*, *J. Immunol.* **149**, 1723 (1992).
7. H. F. Weisman *et al.*, *Science* **249**, 146 (1990).
8. Murine C1q was purified from 50 ml of mouse sera (Sigma, St. Louis, MO) [F. Petry, K. B. M. Reid, M. Loos, *J. Immunol.* **147**, 3988 (1999)]. Briefly, the precipitate from dialysis of serum against 25 mM EGTA, pH 7.5, was resuspended in 0.5 M NaCl, 20 mM EDTA, pH 7.5, and loaded on a Superose 12 column. The positive fractions were then pooled, dialyzed against 20 mM EDTA, 20 mM Hepes, and the precipitate solubilized in SDS sample buffer and separated by SDS-polyacrylamide gel electrophoresis (SDS-PAGE). After staining with Coomassie blue to locate the bands, we excised the C1q bands and used them for immunization. The C1q antigen that was used for protein immunoblotting and for blocking experiments was purified by applying mouse serum (plus 10 mM EDTA) to a BioRex 70 column as described [A. J. Tenner, P. H. Lesavre, N. R. Cooper, *J. Immunol.* **127**, 648 (1981); K. R. Young, J. L. Ambrus Jr., A. Malbran, A. S. Fauci, A. J. Tenner, *ibid.* **146**, 3356 (1991)], followed by ammonium sulfate precipitation.
9. Before giving anesthesia to the mice, we examined them for neurological deficit 23 hours after reperfusion using a four-tiered grading system: 1, the animal demonstrated normal, spontaneous, movements; 2, the animal was noted to be turning toward the ipsilateral side; 3, the animal was observed to spin longitudinally (clockwise when viewed from the tail); and 4, the animal was unresponsive to noxious stimuli. This scoring system has been previously described for mice (2).
10. C. J. M. Frijns *et al.*, *Stroke* **28**, 2214 (1997); Y. Okada *et al.*, *ibid.* **25**, 202 (1994); H. P. Haring, E. L. Berg, N. Tsurushita, M. Tagaya, G. J. del Zoppo, *ibid.* **27**, 1386 (1996).
11. C. W. Rittershaus *et al.*, *J. Biol. Chem.* **274**, 11237 (1999).
12. In an alternative way of measuring tissue injury in stroke, an indirect method of calculating infarct volumes was also used, based on the same TTC-stained serial cerebral sections [R. A. Swanson *et al.*, *J. Cereb. Blood Flow Metab.* **10**, 290 (1990); T. N. Lin, Y. Y. He, G. Wu, M. Kahn, C. Y. Hsu, *Stroke* **24**, 117 (1993)]. The effects of sCR1 and sCR1sLe\* administration on infarction size persisted when the indirect method was used to perform the morphometric analysis of infarcted areas. Pretreatment with sCR1sLe\* resulted in a significant reduction in infarct size from  $11.4 \pm 2.5\%$  to  $1.6 \pm 0.9\%$  ( $P = 0.04$ ), whereas pretreatment with sCR1 had only an intermediate effect on infarct size reduction to  $7.4 \pm 2.2\%$  ( $P =$  not significant). Furthermore, these effects were reproducible in cohorts that received either sCR1 or sCR1sLe\* after the removal of the occluding suture. sCR1sLe\* caused a decrease in infarct size from  $16.6 \pm 4.5\%$  to  $3.7 \pm 1.2\%$  ( $P = 0.02$ ), whereas sCR1 caused an intermediate reduction to  $9.3 \pm 2.7\%$  ( $P =$  not significant). All of the conclusions based on either method remain the same, but the values for the "indirect infarction volumes" are smaller than those for the "direct technique, as has been reported in previous comparisons of the two methods.
13. B. Furie and B. C. Furie, *Thromb. Haemostasis* **74**, 224 (1995); P. H. M. Kuijper *et al.*, *Blood* **87**, 3271 (1996); T. G. Diacovo, S. J. Roth, J. M. Buccola, D. F. Bainton, T. A. Springer, *ibid.* **88**, 146 (1996).
14. J. Huang, L. J. Kim, A. Poisk, D. J. Pinsky, E. S. Connolly Jr., *Neurosurgery*, in press.
15. C. J. Prestigiacomo *et al.*, *Stroke* **30**, 1110 (1999).
16. The administration of sCR1 has not previously been shown to have any adverse effects. In a rat model of hemorrhage and resuscitation, sCR1 had no adverse effects on arterial pressure, heart rate, or cardiac output [T. M. Fruchterman, D. A. Spain, M. A. Wilson, P. D. Harris, R. N. Garrison, *Surgery* **124**, 782 (1998)]. In pigs subjected to cardiopulmonary bypass with or without revascularization of ischemic myocardium, administration of sCR1 had no adverse effects on systemic or pulmonary hemodynamics [A. M. Gillinov *et al.*, *Ann. Thorac. Surg.* **55**, 619 (1993); H. L. Lazar *et al.*, *ibid.* **65**, 973 (1998)]. In our experiments, mice were subjected to administration of either sCR1 or sCR1sLe\*, followed by sternotomy and placement on a rodent ventilator (with room air) for direct sampling of left ventricular blood 3 hours later [vehicle, sCR1 (15 mg/kg), or sCR1sLe\* (15 mg/kg) given as a 200- $\mu$ l intravenous injection; five animals per group]. For each of the three groups (in order), data showed the following: mean arterial oxygenation of  $163 \pm 13$ ,  $141 \pm 12$ , and  $152 \pm 11$  mm Hg,  $P =$  not significant between groups; and serum glucose concentrations were  $326 \pm 21$ ,  $384 \pm 44$ , and  $377 \pm 6$  mg/dl,  $P =$  not significant between groups.
17. D. Chiu *et al.*, *Stroke* **29**, 18 (1998).
18. L. B. Klickstein, S. F. Barbashev, T. Liu, R. M. Jack, A. Nicholson-Weller, *Immunity* **7**, 345 (1997).
19. S. C. Makrides *et al.*, *J. Biol. Chem.* **267**, 24754 (1992).
20. T. F. Choudhri, B. L. Hoh, R. A. Solomon, E. S. Connolly Jr., D. J. Pinsky, *Stroke* **28**, 2296 (1997).
21. We acknowledge the technical assistance of H. Liao and Y. Shan Zou in preparation of tissue for immunohistochemistry, M. Fonseca and G. Palmarini for preparation of murine anti-C1q, and helpful input by T. Choudhri, R. McTaggart, B. Hoh, D. Hoh, and K. Okada. Supported by the Public Health Service (grants R01 HL59488 and R01 HL55397 to D.J.P., and grant R01 NS35144 to A.J.T.). L.J.K. was supported by an American Heart Association and an Alpha Omega Alpha Medical Student Research Award. E.S.C. Jr. participated in this work as part of a Clinical Investigator Development award from the NIH (NS02038), and D.J.P. was supported by a Clinician-Scientist Award from the American Heart Association.

15 March 1999; accepted 21 June 1999

## Correlational Structure of Spontaneous Neuronal Activity in the Developing Lateral Geniculate Nucleus in Vivo

Michael Weliky\*† and Lawrence C. Katz

The properties of spontaneous activity in the developing visual pathway beyond the retina are unknown. Multielectrode recordings in the lateral geniculate nucleus (LGN) of awake behaving ferrets, before eye opening, revealed patterns of spontaneous activity that reflect a reshaping of retinal drive within higher visual stages. Significant binocular correlations were present only when cortico-thalamic feedback was intact. In the absence of retinal drive, cortico-thalamic feedback was required to sustain correlated LGN bursting. Activity originating from the contralateral eye drove thalamic activity far more strongly than that originating from the ipsilateral eye. Thus, in vivo patterns of LGN spontaneous activity emerge from interactions between retina, thalamus, and cortex.

Although visual experience affects visual cortical plasticity during specific critical periods of postnatal development (1), many aspects of visual cortical functional organization emerge before visual experience (2–4). Thus, visual experience is not required for the initial development of cortical functional organization but is necessary for its maintenance and stability.

Before the onset of visual experience, spontaneous activity within the visual pathway has been proposed to provide instructive cues for guiding orientation and ocular dominance column formation within visual cor-

tex. Correlated patterns of spontaneous activity have been observed in the developing retina (5, 6); however, very little is known about the in vivo patterns of spontaneous activity within higher stages of the visual pathway such as the lateral geniculate nucleus (LGN). It is unlikely that the LGN simply relays patterns of retinal spontaneous activity to the cortex; rather, it reshapes and transforms these patterns. Mechanisms that could underlie these transformations include non-retinal sources of input such as cholinergic brainstem afferents (7), massive feedback projections from layer 6 of primary visual cortex (8), and LGN and perigeniculate nucleus (PGN) circuitry, which generates endogenous synchronized network oscillations in vitro (9, 10). The eventual patterns of spontaneous activity that underlie the development of visual cortical functional architecture may be quite different from those predicted by retinal activity alone. To investigate

Howard Hughes Medical Institute and Department of Neurobiology, Duke University Medical Center, Durham, NC 27710, USA.

\*Present address: Department of Brain and Cognitive Sciences, Meliora Hall, University of Rochester, Rochester, NY 14627, USA.

†To whom correspondence should be addressed. E-mail: weliky@cvs.rochester.edu

## REPORTS

whether such transformations occur and the circuitry underlying them, we recorded spontaneous neuronal activity across different

eye-specific and ON/OFF LGN layers in awake behaving ferrets before eye opening. Positioning a multielectrode array along

the parasagittal axis of the LGN enabled recordings from the functionally distinct cell layers of the LGN (Fig. 1, A and B) (11, 12).

**Fig. 1.** Multielectrode recordings from the LGN of neonatal awake behaving ferrets. **(A)** Parasagittal cut through the LGN showing the organization of eye-specific layers A and A1 and their respective ON/OFF sublaminae. Electrodes are spaced 100  $\mu$ m apart. The diagram predicts the progression of A (contralateral) and A1 (ipsilateral) sublamina recorded by the eight electrodes. P, perigeniculate nucleus; C, lamina C. Ant., anterior; Dors., dorsal; Post., posterior; Vent., ventral. **(B)** Spike discharges evoked at the eight electrodes in response to the onset or offset of light flashes to the ipsilateral and contralateral eyes. The progression of functional layers predicted in (A) is observed in the numbered traces. Light flash onset for the ipsilateral eye occurs at 1 s and is offset at 4 s into the recordings. Light flash onset for the contralateral eye occurs at 7 s and is offset at 10 s. **(C)** Synchronous bursts of spontaneous neuronal activity recorded through the eight recording electrodes. The upper traces show functionally discriminated multiunit-single-unit spike activity recorded by each of the eight electrodes. This recording was made just after obtaining the light-evoked responses shown in (B) in the same animal and therefore represents spike activity from the same identified cells. The functional identity of cells recorded by the different electrodes was confirmed by again testing the responses to light flash after recording spontaneous activity for about 1 hour, indicating stability of the recording electrodes. All units fired a 5- to 10-s burst of action potentials beginning at about 15 s. Below the traces, the rate of spike discharge for identified units at each electrode is encoded in gray scale in the time series graph where bright pixels indicate high discharge rate. Bin width, 200 ms. Horizontal rows show the rate of spike discharge for each electrode (electrode 1 is the top row). The bracketed region shows the 40-s time period represented in the upper traces 1 to 8.

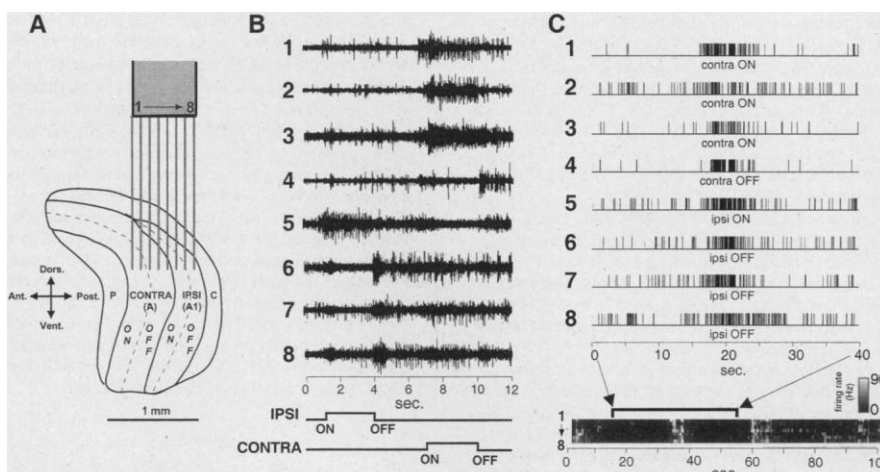
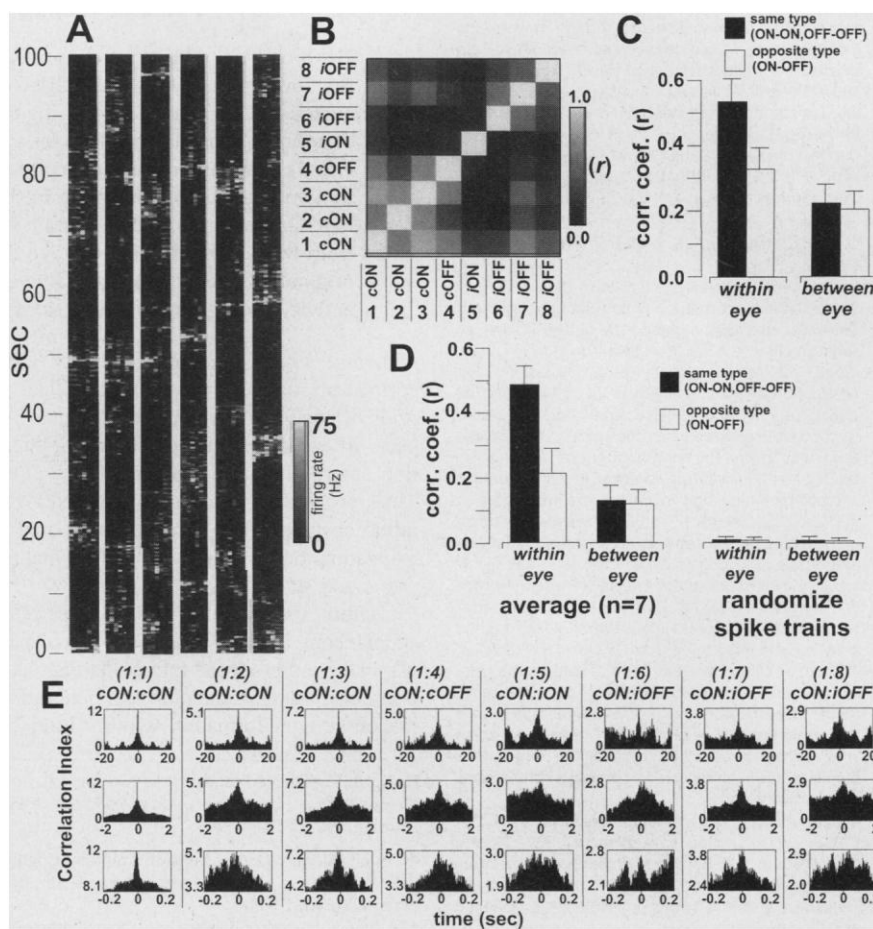


**Fig. 2.** The correlational structure of spontaneous activity in normal animals. **(A)** Time series graphs show periodic, correlated bursts of neuronal activity across the electrode array. Time series graphs are shown for successive 100-s acquisition trials. Average burst frequency = 2.2 bursts/min. In all time series graphs in this and subsequent figures, electrode 1 is the leftmost column of pixels. Bin width, 200 ms. **(B)** Cross-correlation matrix calculated from the same animal shown in (A). Rows and columns are labeled by electrode number (1 to 8) and the functionally identified units recorded by each electrode. Each square located at a column/row intersection is gray scale encoded to represent the amount of correlated activity ( $r$ ) between each pair of electrodes. White represents the highest correlation of 1.0 and black represents a correlation of 0.0. c, contralateral; i, ipsilateral. **(C)** Histogram of the average correlation strength between different LGN eye-specific and ON/OFF layers calculated from the correlation matrix shown in (B). **(D)** (left) Histogram showing average correlation strength between different LGN eye-specific and ON/OFF layers for seven animals. (right) Histogram constructed from the same data used in the control histogram on the left but with all spike trains randomly shifted in time (14). The correlations between randomized spike trains are near 0.0 ( $r = 0.013 \pm 0.008$ ); these are significantly smaller than the correlations calculated from control spike trains ( $P < 0.005$ ,  $t$  test). Error bars in this and subsequent figures show standard deviation. **(E)** Cross-correlation functions calculated between pairs of electrodes lying within different LGN layers. Each column shows the correlation function computed between spikes recorded at electrode 1 and each of the eight electrodes during a single 100-s recording trial [computed from the third time series graph from the left in (A)]. The three rows show the same function at progressively finer time scales. Each column is labeled by the pair of electrodes and corresponding functional layers (c, contralateral; i, ipsilateral) used to compute the cross-correlation function.



## REPORTS

Recordings obtained from ferrets [postnatal ages 24 to 27 ( $n = 7$ )] revealed patterns of spontaneous activity consisting of synchronous bursts of neuronal activity across all LGN layers (Fig. 1C). Burst duration ranged from 8 to 20 s (mean =  $14.5 \pm 4.7$  s) with an interburst interval of 15 to 40 s (mean =  $26.1 \pm 8.9$  s). The average burst frequency was 2.3 bursts/min. Recordings were reliably obtained from individual animals for 1 to 3 days and did not show significant alterations in burst patterns over this time. Activity patterns were similar during periods of quiet resting or active exploratory behavior.

The dynamics of neuronal activity record-

ed across the electrode array were revealed by constructing time series graphs (Figs. 1C and 2A). Cell activity during a burst was not strictly simultaneous at all electrodes (Fig. 2A). In some cases, activity at one set of electrodes preceded activity at other electrodes; in other cases, discharge rates or temporal firing patterns varied among the electrodes. To assess systematic differences in correlated firing between different LGN cell types, we calculated Pearson product correlation coefficients ( $r$ ) between spike trains recorded by all pairs of electrodes (Fig. 2B) (13). For all cross-correlation calculations, spikes were binned into 260-ms bins. Corre-

lation histograms were also constructed from spike trains in which spikes were binned into different size bins ranging from 20 to 260 ms. The pattern of layer-specific correlations remained the same at the different binned time scales.

All pair-wise cross correlations were averaged into four groups according to whether each electrode pair recorded activity from the same or different eye-specific layers (ipsilateral/contralateral) and the same or opposite center-type layers (ON/OFF) (Fig. 2, C and D). These cross correlations reveal systematic differences in the levels of correlated activity between different eye-specific and ON/OFF layers. The activity of neurons from the same eye and same center-type layer (for example, contra-ON/contra-ON) was most highly correlated ( $r = 0.485 \pm 0.051$ ), whereas correlations between neurons from the same eye but opposite center-type layer (for example, contra-ON/contra-OFF) were about half as strong ( $r = 0.216 \pm 0.075$ ). These layer-specific differences in correlated activity were all statistically significant ( $P < 0.05$ ,  $t$  test).

Because no direct connections link the two eyes, and if each retina independently generated spontaneous bursts of activity, there should be essentially no correlation between the patterns of spontaneous activity originating from the two eyes. However, neurons from different eye-specific LGN layers were significantly correlated ( $r = 0.135 \pm 0.049$ ) (Fig. 2, C and D). Although weaker than the correlations within each eye-specific layer, these correlations were far higher than what would be expected by chance if cells within different eye-specific layers burst independently ( $P < 0.005$ ,  $t$  test) (Fig. 2D) (14). The correlations between different eye-specific layers having the same or opposite receptive field center type were equally strong ( $P > 0.05$ ,  $t$  test) (Fig. 2, C and D). The pattern of correlated bursting activity within ON and OFF LGN layers differed from the predictions of in vitro retinal recording. In vitro recordings, carried out in retinas obtained from animals of similar age to those used in our LGN recordings, have shown that the interval between ON retinal ganglion cell bursts is about 30 s, whereas the interval between OFF retinal ganglion cell bursts is about 90 s (6). However, the in vivo burst frequency of cells within ON and OFF LGN layers was similar: Individual ON and OFF layers both showed autocorrelation peaks close to 25 s.

One explanation for the pattern of correlations is that it reflects the distance between recording electrodes, with correlated activity declining with increasing distance between recording sites. If this were the case, then correlations within the same eye-specific layer would be highest because these recording sites

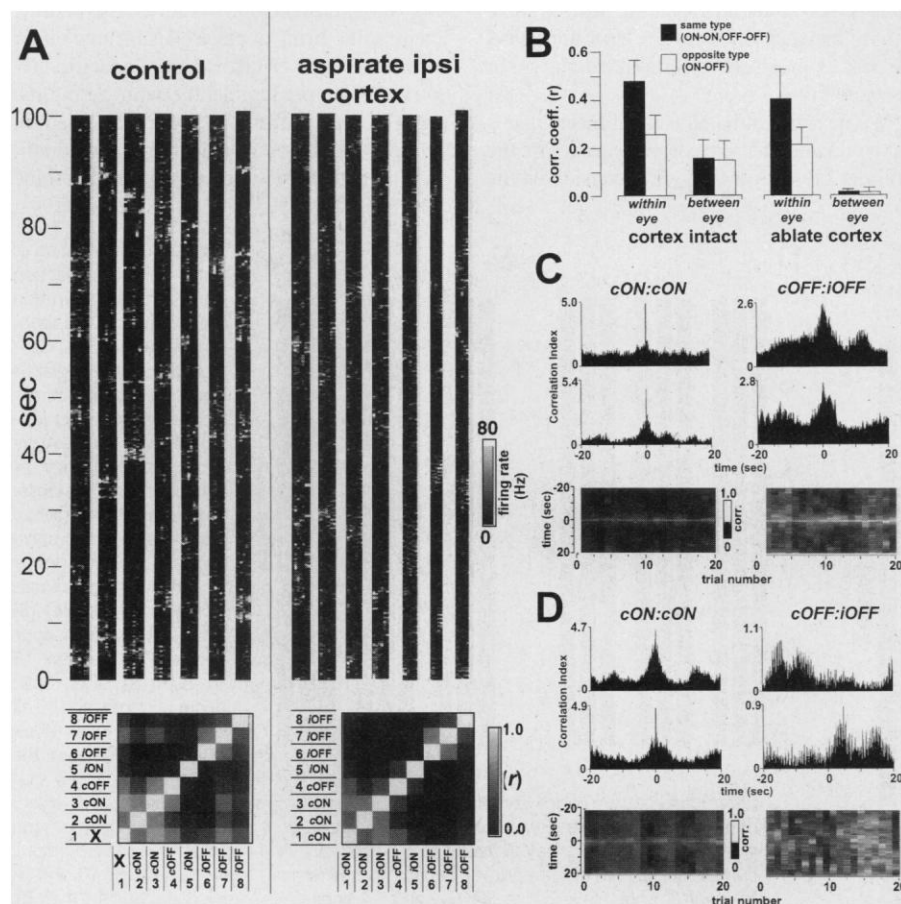


**Fig. 3.** Feedback from the visual cortex mediates binocular correlations in LGN spontaneous activity. (A) The effect of aspirating the ipsilateral cortex on the pattern of LGN spontaneous activity. (left) The time series graphs were obtained with intact ipsilateral visual cortex. The resulting cross-correlation matrix is shown below the time series graphs. (right) After aspiration of the ipsilateral visual cortex, the cross-correlation matrix reveals that although within-eye correlations remain unchanged, between-eye correlations disappear. Bin width, 200 ms (all time series graphs). (B) Summary of results from three animals. With visual cortex intact, significant correlations between different eye-specific layers are present; after cortical ablation, these correlations disappear. (C) With intact visual cortex, cross-correlation functions calculated between electrodes located within the same eye-specific layer (contralateral eye/ON) (left) and different eye-specific layers (contralateral/OFF and ipsilateral/OFF) (right). The upper two histograms in each column show representative cross-correlation functions. The lower graph shows a series of 20 normalized cross-correlation functions calculated for successive 100-s recording trials. Gray scale encodes the normalized number of binned spikes from black (0.0) to white (1.0). The white horizontal line seen at the 0.0 time position in both graphs indicates strong correlations with zero time lag. (D) Same as (C) but after cortical ablation. Although strong correlations occur with zero time lag between electrodes located within the same eye-specific layer, peaks in the cross-correlation functions calculated between the different eye-specific layers occur at random positions.

## REPORTS

are nearby, whereas correlations between different eye-specific layers would be weakest because, on average, these sites are more distant from one another (Fig. 1A). To rule out this possibility, we calculated cross correlations only between adjacent electrodes or between electrodes separated by one intervening electrode. In all cases, the same pattern of correlations was observed. If adjacent electrodes were located in different eye-specific layers, their correlation coefficients were low, whereas if they were located in the same eye-specific layer, the correlations were much stronger. Thus, interelectrode spacing does not dictate the levels of correlated activity.

To investigate how the timing of spike activity between different LGN layers could underlie the computed pattern of correlation coefficients, we calculated cross-correlation functions between pairs of spike trains during each 100-s recording trial (Fig. 2E) (15). The normalized amplitudes of these functions were consistent with the Pearson product cor-

relation coefficients calculated between the different layers. Typically, these functions showed the strongest correlations occurring with zero time lag within the same as well as between different layers. However, at fine time scales, single as well as multiple peaks were observed at nonzero phase positions with greater frequency in cross-correlation functions computed between different eye-specific layers than within the same eye-specific layer. Cross-correlation functions calculated between different eye-specific layers tended to have wider central peaks, as well as to exhibit a higher degree of asymmetry both in the distribution of individual peaks and in the amplitude of the flanks of these peaks. Thus, at fine time scales, spike activity between different eye-specific layers was not as precisely synchronized as within the same layer.

We next investigated several mechanisms that could generate the correlations across the different LGN layers. We first considered the

circuits that could underlie the generation of binocular responses. One candidate is the large feedback connection from layer 6 of visual cortex to the LGN (8, 16). To test this connection, we ablated the ipsilateral visual cortex while retinal input to the LGN was maintained ( $n = 3$  animals) (17). Although this did not substantially alter the overall temporal pattern of LGN bursting or the correlated activity within the same eye-specific layer, correlated activity across different eye-specific layers was eliminated (Fig. 3, A and B). After removal of cortical feedback, correlation coefficients calculated between electrodes located within different eye-specific layers were indistinguishable from random ( $P > 0.05$ ,  $t$  test) (14). With the visual cortex intact, spike firing at electrodes located either within the same or different eye-specific layers occurred predominantly with zero time lag (Fig. 3C). After visual cortical ablation, strong correlations in spike firing were still present with zero time lag within the same

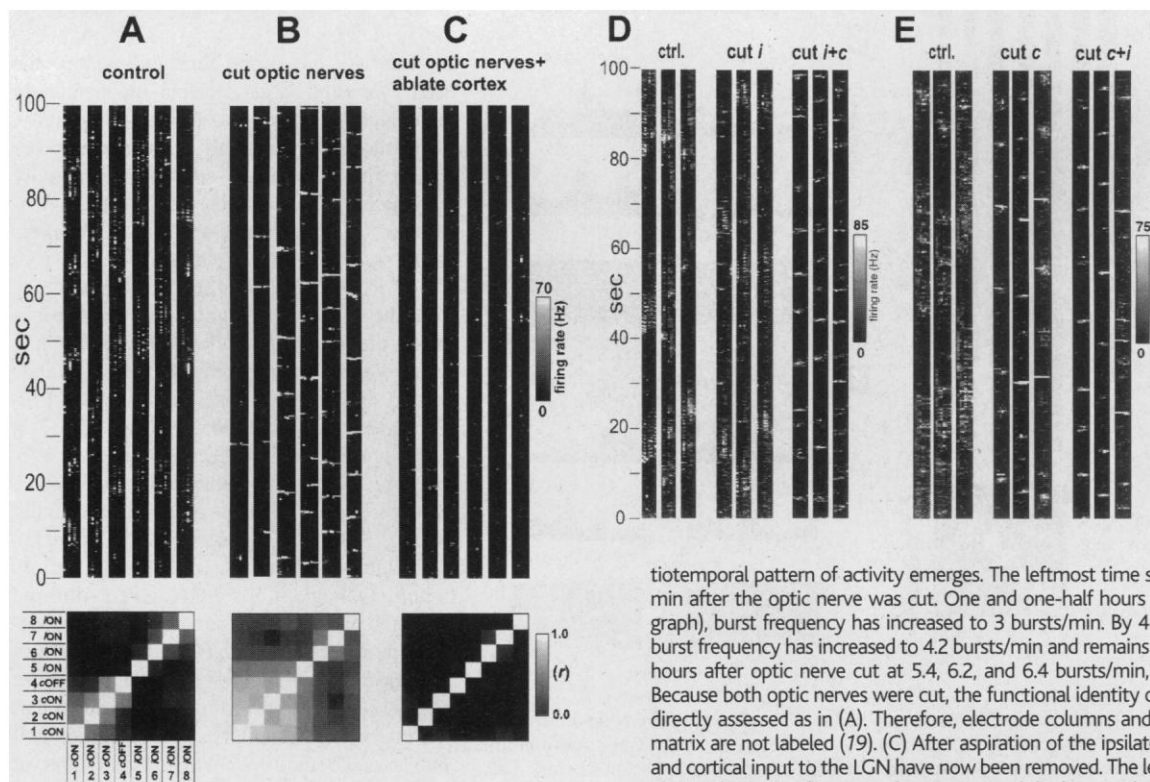


**Fig. 4.** (A to C) Effects of optic nerve transection and cortical aspiration on patterns of LGN spontaneous activity. (A) Control time series graphs obtained with intact optic nerves and intact ipsilateral visual cortex. Average burst frequency = 2.1 bursts/min. The cross-correlation matrix (below the time series graphs) shows a pattern similar to other control animals (for example, Fig. 2B). (B) After cutting both optic nerves. For the first 15 to 30 min after optic nerve transection, all LGN activity was abolished. Gradually over the next 6 hours, a new spatiotemporal pattern of activity emerges. The leftmost time series graph shows activity 45 min after the optic nerve was cut. One and one-half hours after optic nerve cut (second graph), burst frequency has increased to 3 bursts/min. By 4 hours after cut (third graph), burst frequency has increased to 4.2 bursts/min and remains relatively stable 6, 10, and 16 hours after optic nerve cut at 5.4, 6.2, and 6.4 bursts/min, respectively (graphs 4 to 6). Because both optic nerves were cut, the functional identity of recorded units could not be directly assessed as in (A). Therefore, electrode columns and rows in the cross-correlation matrix are not labeled (19). (C) After aspiration of the ipsilateral visual cortex. Both retinal and cortical input to the LGN have now been removed. The leftmost time series graph was obtained 10 min after cortical aspiration and the last graph 18 hours after aspiration. The

cross-correlation matrix shows the almost complete absence of correlated activity when compared with the matrices in (A) and (B). (D and E) Contralateral eye bias in driving spontaneous LGN activity. (D) Time series graphs obtained from successive transection of the optic nerves in a single animal. (left) Time series graphs with both optic nerves intact. Electrodes 1 to 4 were recorded from the contralateral layer and electrodes 5 to 8 from the ipsilateral layer. Average burst frequency = 1.7 bursts/min. (middle) Time series graphs obtained after ipsilateral (*i*) optic nerve cut. The first and last graphs were obtained 20 min and 10 hours, respectively, after optic nerve cut. Average burst frequency = 1.9 bursts/min. Spontaneous activity was observed on electrodes 5 to 8 even though these units could not be driven by light flash to either eye. (right) Time series graphs obtained after contralateral (*c*) optic nerve cut. Retinal input to the LGN from both optic nerves has now been completely removed. The first and last graphs were obtained 15 min and 11 hours, respectively, after optic nerve cut. Average burst frequency = 6.5 bursts/min. (E) Time series graphs obtained from successive transection of the optic nerves in a second individual animal. Optic nerves were cut in reverse order from the animal shown in (D). (left) Time series graphs obtained with both optic nerves intact. Electrodes 1 to 4 were recorded from the contralateral layer and electrodes 5 to 8 from the ipsilateral layer. Average burst frequency = 1.3 bursts/min. (middle) Time series graphs obtained after contralateral (*c*) optic nerve cut. Average burst frequency = 4.7 bursts/min. The first and last graphs were obtained 25 min and 12 hours, respectively, after optic nerve cut. Spontaneous activity was seen on electrodes 1 to 4 even though these units could not be driven by light flash to either eye. (right) Time series graphs obtained after ipsilateral (*i*) optic nerve cut. Retinal input to the LGN from both optic nerves has now been completely removed. Average burst frequency = 5.1 bursts/min. The first and last graphs were obtained 20 min and 14 hours, respectively, after optic nerve cut. Bin width, 200 ms (all time series graphs).

cross-correlation matrix shows the almost complete absence of correlated activity when compared with the matrices in (A) and (B). (D and E) Contralateral eye bias in driving spontaneous LGN activity. (D) Time series graphs obtained from successive transection of the optic nerves in a single animal. (left) Time series graphs with both optic nerves intact. Electrodes 1 to 4 were recorded from the contralateral layer and electrodes 5 to 8 from the ipsilateral layer. Average burst frequency = 1.7 bursts/min. (middle) Time series graphs obtained after ipsilateral (*i*) optic nerve cut. The first and last graphs were obtained 20 min and 10 hours, respectively, after optic nerve cut. Average burst frequency = 1.9 bursts/min. Spontaneous activity was observed on electrodes 5 to 8 even though these units could not be driven by light flash to either eye. (right) Time series graphs obtained after contralateral (*c*) optic nerve cut. Retinal input to the LGN from both optic nerves has now been completely removed. The first and last graphs were obtained 15 min and 11 hours, respectively, after optic nerve cut. Average burst frequency = 6.5 bursts/min. (E) Time series graphs obtained from successive transection of the optic nerves in a second individual animal. Optic nerves were cut in reverse order from the animal shown in (D). (left) Time series graphs obtained with both optic nerves intact. Electrodes 1 to 4 were recorded from the contralateral layer and electrodes 5 to 8 from the ipsilateral layer. Average burst frequency = 1.3 bursts/min. (middle) Time series graphs obtained after contralateral (*c*) optic nerve cut. Average burst frequency = 4.7 bursts/min. The first and last graphs were obtained 25 min and 12 hours, respectively, after optic nerve cut. Spontaneous activity was seen on electrodes 1 to 4 even though these units could not be driven by light flash to either eye. (right) Time series graphs obtained after ipsilateral (*i*) optic nerve cut. Retinal input to the LGN from both optic nerves has now been completely removed. Average burst frequency = 5.1 bursts/min. The first and last graphs were obtained 20 min and 14 hours, respectively, after optic nerve cut. Bin width, 200 ms (all time series graphs).

eye-specific layer but not between different eye-specific layers (Fig. 3D). In the absence of cortical feedback, the largest peaks in cross-correlation functions calculated between different eye-specific layers were typically shifted to random locations, ranging from  $\pm 1$  to 15 s, during successive 100-s recording trials. Such shifts underlie the marked reduction of cross-correlation coefficients ( $r$ ) computed between different eye-specific layers after cortical ablation (Fig. 3B). This reduction indicates that cortical feedback is required to synchronize neuronal activity between the different eye-specific LGN layers.

Correlations between different eye-specific layers, as well as the common burst frequency of ON and OFF center cells, could also be produced by synchronized LGN and PGN oscillatory activity (9, 10) or by neuromodulatory inputs from the brainstem (7). We transected both optic nerves to remove retinal afferent drive to the LGN while leaving cortical feedback connections (and brainstem afferents) intact ( $n = 5$  animals) (Fig. 4, A and B) (18). This markedly changed the spatiotemporal pattern of LGN activity. After an initial period of suppressed activity, average burst frequency increased from 2.3 bursts/min before transection to 6.1 bursts/min 6 hours after transection. Burst duration decreased from 8 to 20 s before to 1 to 2 s after transection, and the level of correlated activity averaged across all electrodes increased from 0.23 before to 0.49 after transection. The level of correlated activity after optic nerve transection did not increase uniformly between all electrodes: Electrodes within the presumptive contralateral eye-specific layer appeared to be most highly correlated, with weaker correlations between the ipsilateral and contralateral layers as well as within the ipsilateral layer itself (Fig. 4B) (19).

The pattern of spontaneous activity observed in the absence of retinal inputs could be due to a number of mechanisms such as intrinsic LGN/PGN bursting alone (9, 10), contributions from brainstem afferents (7), or activity within reciprocal connections between thalamus and cortex (20). To distinguish between these possibilities in the animals with transected optic nerves, we subsequently ablated the ipsilateral visual cortex ( $n = 3$  animals). In all cases, this ablation completely abolished bursting activity (Fig. 4C). Spontaneous activity within the LGN consisted solely of random and uncoordinated spikes across different electrodes. Correlated activity averaged across all electrodes decreased from 0.49 to 0.07 after cortical ablation. In the absence of retinal input, cortico-thalamic feedback is required to sustain synchronized LGN and PGN oscillatory activity in vivo. At these early ages, the LGN alone, or in conjunction with brainstem afferents, can-

not sustain patterned bursting activity.

Cortical inputs regulate LGN spontaneous activity differently than retinal inputs. This difference may arise from the different pattern of projections that retinal and cortical inputs make within the LGN and PGN: Cortical feedback inputs innervate both the PGN and LGN and, unlike retinal afferents, do not distinguish between LGN layers (16), whereas retinal inputs only innervate the LGN. Furthermore, retinal and cortical inputs activate different metabotropic glutamate receptors (21). The cortex could regulate LGN bursting activity through the PGN, whose neurons form strong inhibitory synapses onto LGN neurons (22, 23). Additionally, the cortex primarily exerts a strong modulatory effect on spindle wave production and synchronization (20), and the retina directly drives LGN neuronal activity through ganglion cell bursting (24).

Optical imaging and single-unit recordings demonstrate a contralateral eye dominance in driving cortical orientation and ocular dominance responses before eye opening (3, 25). To explore whether this eye dominance could arise from an early biasing of eye-specific activity within the developing LGN, we compared the effects of separate ipsilateral or contralateral optic nerve transection on LGN spontaneous activity ( $n = 6$ ). Transection of only the ipsilateral optic nerve had a negligible effect on the pattern of LGN bursting (Fig. 4D). Subsequent transection of the remaining contralateral optic nerve changed LGN activity to the pattern of short, highly coherent bursts described above after simultaneous transection of both optic nerves. Reversing the order of the cuts and transecting the contralateral optic nerve first produced a different effect on the pattern of LGN spontaneous activity (Fig. 4E). After transection of the contralateral optic nerve alone, LGN activity changed to the pattern of short, highly coherent bursts observed when both optic nerves were cut. Subsequent transection of the ipsilateral optic nerve produced no additional alteration in the pattern of LGN bursting. Thus, normal LGN spontaneous activity is strongly biased by contralateral eye drive. Bursting activity by the ipsilateral eye, which would typically arrive out of phase with bursts produced by the contralateral eye, may be actively suppressed by intrinsic LGN and PGN inhibitory circuitry (9, 10, 22, 23). If this is true, activity within the ipsilateral eye-specific layer may be primarily generated by thalamo-cortical circuits, triggered by contralateral retinal activity.

The coupling of multiple mechanisms, including endogenous network oscillations and thalamo-cortical feedback, produces emergent patterns of spontaneous activity within the LGN. The resulting correlational structure of LGN spontaneous activity could provide instructive cues for guiding the estab-

lishment of adult patterns of synaptic connectivity within the visual pathway. Several features of the correlational structure of LGN spontaneous activity are consistent with predictions of activity-dependent models of cortical map and receptive field development. Modeling studies propose that differences in correlated firing between ON and OFF LGN afferents, similar to those experimentally observed, can drive the segregation of simple cell ON/OFF subregions (26). Theoretical models also demonstrate that the competing requirements of joint ocular dominance and orientation map development can be resolved by biasing the pattern of correlated activity between the two eyes (27). Ocular dominance and orientation preference maps will jointly develop if within-eye activity is more highly correlated than between-eye activity, which is what was observed experimentally. However, certain central features of our results are difficult to incorporate into existing models. The strong contralateral bias observed experimentally does not appear consistent with standard formulations for the role of patterned activity in ocular dominance column formation (28). Taken together with previous work showing a contralateral bias in cortical development (3, 25), these results challenge the idea that ipsilateral and contralateral geniculocortical projections start out on an equal footing.

Binocular enucleation at postnatal age 21 in ferrets only modestly affects the development of clustered horizontal connections in the cortex whereas silencing the cortex abolishes clusters (29). These findings suggest that in animals in which both optic nerves were transected, thalamo-cortical network activity can sustain or guide the formation of clustered horizontal connections in enucleated animals. Thus, even in the absence of retinal drive, activity in the thalamo-cortical loop may contain information that can drive the initial patterning of cortical circuits and visual cortical functional architecture.

#### References and Notes

1. T. N. Wiesel and D. H. Hubel, *J. Neurophysiol.* **26**, 978 (1963); *ibid.*, p. 1003; D. H. Hubel and T. N. Wiesel, *J. Physiol.* **206**, 419 (1970); S. LeVay, *Philos. Trans. R. Soc. London Ser. B* **278**, 377 (1977); J. D. Pettigrew, *J. Physiol.* **237**, 49 (1974); B. Chapman and M. P. Stryker, *J. Neurosci.* **13**, 5251 (1993); M. C. Crair, E. S. Ruthazer, D. C. Gillespie, M. P. Stryker, *Neuron* **19**, 307 (1997).
2. T. N. Wiesel and D. H. Hubel, *J. Neurophysiol.* **26**, 994 (1963); *J. Comp. Neurol.* **158**, 307 (1974); P. Rakic, *Philos. Trans. R. Soc. London Ser. B* **278**, 245 (1977); B. Chapman, M. P. Stryker, T. Bonhoeffer, *J. Neurosci.* **16**, 6443 (1996).
3. M. C. Crair, D. C. Gillespie, M. P. Stryker, *Science* **279**, 566 (1998).
4. J. C. Horton and D. R. Hocking, *J. Neurosci.* **16**, 1791 (1996).
5. L. Maffei and L. Galli-Resta, *Proc. Natl. Acad. Sci. U.S.A.* **87**, 2861 (1990); M. Meister, R. O. L. Wong, D. A. Baylor, C. J. Shatz, *Science* **252**, 939 (1991); R. O. L. Wong, M. Meister, C. J. Shatz, *Neuron* **11**, 923 (1993).

6. R. O. L. Wong and D. M. Oakley, *Neuron* **16**, 1087 (1996).

7. B. Hu, M. Steriade, M. Deschenes, *Neuroscience* **31**, 13 (1989); S. M. Lu, W. Guido, S. M. Sherman, *Vis. Neurosci.* **10**, 631 (1993); P. C. Murphy, D. J. Uhrlich, N. Tamamaki, S. M. Sherman, *ibid.* **11**, 781 (1994).

8. H. Hollander, *Brain Res.* **41**, 464 (1972).

9. T. Bal, M. von Krosigk, D. A. McCormick, *J. Physiol.* **483**, 665 (1995).

10. D. A. McCormick, F. Trent, A. S. Ramoa, *J. Neurosci.* **15**, 5739 (1995).

11. The laminar identity of cells recorded by each electrode was determined by affixing small lights, housed within an opaque housing, in front of each eyelid, which were alternately flashed while recording evoked spike discharges. Typically, the microwire electrodes recorded large-amplitude multiunit or single-unit spike activity from one layer, together with smaller amplitude spike activity originating from an adjacent layer. For each electrode, amplitude discrimination techniques reliably isolated neuronal activity originating from the functional layer that produced the largest amplitude spikes. The functional identity of cells was assessed every 30 to 90 min with light flashes to each eye throughout the recording period. This assessment ensured that any slow shifts in recording positions that might recruit new cells from different functional layers would be identified (19). The cells identified during each light flash test session were used to discriminate spikes from subsequent spontaneous activity recordings until the next test session. Spike discrimination was accomplished with a custom LABVIEW program. Typically, each discrimination test session consisted of 8 to 15 light flash sequences, where each sequence consisted of one light flash to each eye (see Fig. 1B). The discrimination procedure was carried out independently at each electrode by first simultaneously displaying evoked spike trains from all light flash sequences from the test session on a computer display. Cursors could be moved up and down simultaneously on all spike train displays representing a single voltage threshold level. Spikes having an amplitude greater than this level were accepted by the program, and a poststimulus time histogram (PSTH) was constructed from all flash sequences and displayed. A spike amplitude threshold was established for each electrode by adjusting the voltage level until the PSTH showed that all accepted spikes were evoked by either light flash onset or offset to only one eye. These voltage levels were subsequently used to discriminate spikes from each electrode until the next discrimination test session.

12. Animals were anaesthetized with a mixture of ketamine hydrochloride [40 mg/kg intramuscularly (i.m.)] and xylazine hydrochloride (2 mg/kg i.m.) and placed in a stereotaxic holder. A 4 mm by 4 mm section of skull was removed and centered at 5 mm posterior to bregma and 5 mm lateral to the midline, and the exposed dura was reflected. The LGN surface was visually exposed by aspirating a 1- to 2-mm bore hole, centered within the region of exposed cortex, vertically through the brain with a small-diameter blunt syringe needle. A single recording electrode was used to first determine the location and size of the

small region of ipsilaterally projecting retinal input with miniature light bulbs, placed in front of each eye, which were alternately flashed, and the response type of recorded neurons (that is, ON/OFF, ipsilateral/contralateral eye) was assessed. The single recording electrode was removed, and the multielectrode array, attached to the headset, was lowered superficially (100 to 200 μm) into the LGN such that roughly half of the eight recording electrodes were within the region of ipsilaterally projecting retinal input. The bore hole was filled with agar to immobilize the LGN and surrounding tissue, and the headset was affixed to the skull with dental acrylic. The multielectrode array consisted of eight 12.5-μm diameter insulated tungsten wires (California Fine Wire, Grover Beach, CA) spaced 100 μm apart in a single row and cut to the same length. The electrodes were glued to a 1-mm-wide shaft of 50-μm-thick tungsten sheet, which was in turn affixed to small plate within the metal headset. The plate could be moved up and down by turning a 4 threads/mm screw, thereby raising or lowering all electrodes simultaneously. During recording, animals were free to move within a low-walled small plastic box placed on a heating blanket. All recordings of spontaneous activity were performed in a dark room. 0.45-m-long small-diameter low-noise coaxial cables connected the animal's headset to custom-made first-stage amplifiers providing 40,000 gain. Two-stage RC circuits bandpass filtered the signal between 600 and 6000 Hz. The amplifiers were mounted above the animal to provide freedom of movement within the box. The amplifiers output was fed into a PC plug-in A/D board (National Instruments, Austin, TX) and digitized at 10 kHz. The acquisition was controlled through custom software written in LABVIEW.

13. The Pearson product correlation coefficient  $r$ , defined by

$$r = \frac{\sum(X - \bar{X})(Y - \bar{Y})}{\sqrt{\sum(X - \bar{X})^2 \sum(Y - \bar{Y})^2}}$$

describes the strength of the association between two variables. Values of  $r$  range from -1.0 to 1.0. Points in  $X$  represent binned spike counts (bin size ranging from 20 to 260 ms) at successive time points (time interval equals the bin size) during a 100-s recording for one electrode. Points in  $Y$  represent the corresponding binned spike counts at a second electrode. This cross-correlation coefficient provides a normalized measurement of the covariance of spike firing rates independent of levels of neuronal activity.

14. At each electrode, binned spikes within each 100-s trial were shifted forward in time a random amount (from 0 to 100 s). Spikes that were shifted beyond the 100-s time point were wrapped around to time 0 +  $t$ . Correlation coefficients were calculated between shifted spike trains for all electrode pairs. For each 100-s trial, spike trains were shifted 100 times, and an average correlation coefficient was obtained for each electrode pair.

15. The cross-correlation function between spike trains recorded at two electrodes was calculated by computing all time intervals between a spike at one

electrode and a spike at the second electrode during a 100-s recording trial, binned into successive 2-ms time bins. The result was divided by the total number of spikes from the first electrode and the bin width. This yields a histogram of the spike firing rate at electrode 2 as a function of time since a spike from electrode 1. This result was normalized by dividing by the total number of spikes from the second electrode and multiplying it by a scale factor of 1000.

16. P. C. Murphy and A. M. Silito, *J. Neurosci.* **16**, 1180 (1996).

17. Animals were anaesthetized by freely breathing a mixture of 2:1 nitrous oxide:oxygen, supplemented by 2.0 to 4.0% Halothane. The posterior region of occipital cortex, about 10 mm by 6 mm, was aspirated with a small-diameter blunt syringe needle. The resulting void was filled with sterile gel foam.

18. The connective tissue and muscles attaching the eyeball to the orbit were cut away. Fine scissors were used to reach behind the eyeball and cut the optic nerve. The rear portion of the eyeball was rotated into view to visually confirm optic nerve transection.

19. After transection of both optic nerves, the functional identity of cells recorded by each electrode could not be directly assessed with light flashes. However, in experiments in which only one optic nerve was cut, almost all electrodes recorded from the same functional layers driven by the intact eye both before and after the surgery, although shifts were occasionally observed at electrodes near layer boundaries. Furthermore, although slow gradual shifts between adjacent layers were also found to occur at electrodes over extended recording periods of 10 to 24 hours, electrodes typically recorded from the same eye-specific and ON/OFF layers. Therefore, we did not label the identity of units recorded after transection of both optic nerves (see Fig. 4, B and C); however, it is likely that most electrodes were still recording from the same LGN layers.

20. D. Contreras, A. Destexhe, T. J. Sejnowski, M. Steriade, *Science* **274**, 771 (1996); D. A. Coulter and C. J. Lee, *Brain Res.* **631**, 137 (1993); C. Q. Kao and D. A. Coulter, *J. Neurophysiol.* **77**, 2661 (1997).

21. D. W. Godwin et al., *J. Neurosci.* **16**, 8181 (1996).

22. F. S. Lo and S. M. Sherman, *Exp. Brain Res.* **100**, 365 (1994).

23. U. Kim, M. V. Sanchez-Vives, D. A. McCormick, *Science* **278**, 130 (1997).

24. R. Mooney, A. A. Penn, R. Gallego, C. J. Shatz, *Neuron* **17**, 863 (1996).

25. I. Godecke, D. S. Kim, T. Bonhoeffer, W. Singer, *Eur. J. Neurosci.* **9**, 1754 (1997).

26. K. D. Miller, *J. Neurosci.* **14**, 409 (1994).

27. E. Ervin and K. D. Miller, *ibid.* **18**, 9870 (1998).

28. N. V. Swindale, *Proc. R. Soc. London Ser. B Biol. Sci.* **208**, 243 (1980); K. D. Miller, J. B. Keller, M. P. Stryker, *Science* **245**, 605 (1989).

29. E. S. Ruthazer and M. P. Stryker, *J. Neurosci.* **16**, 7253 (1996).

30. L.C.K. is an Investigator of the Howard Hughes Medical Institute. Also supported by grants from the NIH (National Eye Institute).

17 September 1998; accepted 9 June 1999

## Enhance your AAAS membership with the Science Online advantage.

- **Full text Science**—research papers and news articles with hyperlinks from citations to related abstracts in other journals before you receive *Science* in the mail.
- **ScienceNOW**—succinct, daily briefings, of the hottest scientific, medical, and technological news.
- **Science's Next Wave**—career advice, topical forums, discussion groups, and expanded news written by today's brightest young scientists across the world.

**Science ONLINE**

- **Research Alerts**—sends you an e-mail alert every time a *Science* research report comes out in the discipline, or by a specific author, citation, or keyword of your choice.
- **Science's Professional Network**—lists hundreds of job openings and funding sources worldwide that are quickly and easily searchable by discipline, position, organization, and region.
- **Electronic Marketplace**—provides new product information from the world's leading science manufacturers and suppliers, all at a click of your mouse.

All the information you need...in one convenient location.

Visit Science Online at <http://www.sciencemag.org>, call 202-326-6417, or e-mail [membership2@aaas.org](mailto:membership2@aaas.org) for more information.

AAAS is also proud to announce site-wide institutional subscriptions to Science Online. Contact your subscription agent or AAAS for details.



AMERICAN ASSOCIATION FOR THE ADVANCEMENT OF SCIENCE